Building An Ecological Port Loading Bunker to Mitigate Environmental Pollution in Maritime Transport

Özge Güler*
Burçelik Bursa Çelik Döküm Sanayi A.Ş.
Bursa/TÜRKİYE

Mustafa Cemal Çakır
Bursa Uludağ Üniversitesi
Makine Mühendisliği Bölümü
Bursa/TÜRKİYE

Makale Bilgisi:
Araştırma Makalesi
Gönderilme: 1 Ekim 2025
Kabul: 14 Mart 2026

*Sorumlu yazar: Özge Güler
E-mail: ozge.guler@burcelik.com.tr

DOI: https://doi.org/10.56193/matim.1793963

This study analyses the 100 m³ 'Ecological Port Loading Bunker,' a novel development in Turkey with the objective of addressing environmental pollution associated with bulk material logistics in ports, exacerbated by globalization. It also seeks to minimize material waste and ensure safe transportation processes. The calculations pertaining to the bunker at Samsun port are outlined; finite element analyses concerning the structural rigidity of the construction are elaborated, and field activities are corroborated through multiple engineering studies. Theoretical calculations were supplemented by FEM (Finite Element Method) analyses to assess the static behavior of the bunker and its response to dynamic loads. This study included an evaluation of the system's dynamic performance through modal analysis, as well as combined design, shear, and deflection controls for the steel columns and beams within the structural frame. The analysis involved examining the ratio of the maximum values of the relative load combinations to the limit values, revealing that this ratio was consistently below 1 for all columns and beams. The results indicate that the developed ecological port loading bunker has been theoretically validated and is a safe structural element in the field.

Keywords: Port Bunker; Finite Elements; Port Operations; Green Port; European Green Deal

1. INTRODUCTION

Materials such as coal, iron ore, nickel ore, and phosphate are usually transported by sea in powdered and granulated forms. During shipment at ports, products stored in piles produce large amounts of dust under the influence of wind or during transport, causing environmental pollution, damage to the natural habitats of living creatures in the surrounding area, and negative effects on ecological resources in the vicinity. Olaf Merk, Director of Ports and Maritime Transport at the International Transport Forum (ITF) of the OECD, has asserted that the only ports capable of sustaining essential operations in the future are smart ports that optimize space, financial resources, time, and natural resources [1]. This study presents the development of an ecological port loading bunker aimed at mitigating environmental pollution in ports, reducing material waste, and enhancing logistics efficiency.

While direct environmental impact assessment (EIA) reports or academic papers on Ecohoppers are rare, numerous studies exist regarding the overall environmental advantages of dust control technology. Ecohoppers exemplify a direct application of these major benefits. Sources like Environmental Impact Assessment [2] and Baseline Monitoring in Environmental Impact Assessment (EIA) emphasize the significance of EIA procedures and air quality monitoring criteria. Ecohoppers positively influence

assessments by diminishing particulate matter (PM10, PM2.5) emissions.

Yorulmaz et al. [3] conducted studies on sustainability aimed at minimizing the environmental impacts of port operations, which serve as a critical link in international freight transport, as evidenced by a review of national and international publications. Mısır et al. [4] examined the lateral loads induced by wind and wave loads, along with those occurring during ship berthing and mooring, in the context of port design. They simulated the actual lateral load-displacement behavior utilizing Plaxis 3D finite element software. The analyses accurately represented the lateral load-displacement behavior of the piles observed during the loading test. Yılmaz [5] conducted a study estimating wind, Coriolis force, wave, tidal, and density-driven currents in the coastal region of Samsun Bay. He utilized the HYDROTAM-3D three-dimensional hydrodynamic, turbulence, and transport numerical model and validated the results with physical parameters and measurements.

Briassoulis [6] investigated the loads relevant to the design of silos and bunkers, emphasizing the necessity of conducting wind analysis, particularly when the structure is empty and across various sections of the bunker. He supported this assertion by indicating that deformations and buckling are more prevalent at the upper sections of the structure. Aoyama et al. [7] noted that wind loads exhibit local variation, necessitating an assumption for their analysis. Wojcik et al. [8] utilized finite element modeling to analyze the impact of lateral pressure on stresses within the silo during product discharge. Their results indicate that maximum stress is observed during the transition phase, with deformations primarily directed outward. Brown et al. [9] pointed out that two key pressures (pressure against the walls and friction) affect the hopper when products are discharged from the bunker and that it's important to take into account horizontal pressures, stresses, friction, and the weight of the product when designing the hopper. Gençay [10] developed a model under identical conditions and performed analyses utilizing three distinct software programs: STA4-CAD, SAP2000, and İdeCAD. The analyses yielded comparisons of values, including floor weights, earthquake masses, floor irregularities, and vibration periods. The analysis indicated that the program yielded comparable outcomes in key metrics, including irregularities and displacements. The İdeCAD and STA4CAD programs are more user-friendly and practical compared to the SAP2000 program. This advantage is attributed to their integrated menus that support design compliance with regulations and their capacity to quickly calculate and present necessary data, including analysis and measurements.

Shen et al. [11] performed experimental and numerical investigations to quantify the dust concentration in dust suppression hoppers (DSHs) of varying geometries. A scaled test rig was employed to quantify dust concentration, so assessing the dust suppression efficacy of DSHs and identifying the affecting elements. It was noted that the design attributes of the hopper, including the half-angle, outlet opening, and outlet diameter, may substantially influence dust suppression efficacy and dust management. Colinet et al. [12] established through their research that the Dust Suppression Hopper (DSH) diminished airborne respirable dust concentrations by 39% to 88%, as assessed at two sand processing plants by the U.S. National Institute for Occupational Safety and Health (NIOSH). Upon discharge from the hopper, the product manifests as a concentrated column instead of an uncompressed flow, therefore minimizing air entrainment and dust dispersion. Zhang et al. [13] established an experimental model and measuring system for grab discharge utilizing coal, sand, and flour, wherein the interactions among particles, dust, and airflow throughout the discharge process were analyzed in more depth. They assessed the dust dispersion range, velocity and direction of dispersion, settling time, dust concentration, and induced wind speed at several measurement locations. Vaicis et al. [14] examined the particle flow via the hopper nozzle under varying settings based on vibration frequency. A frequency analysis of the dust hopper was conducted using a basic FEM model.

Upon examination of national and international patents in the research, it was noted that patent no. [CN 2022/115180431A] pertains to an unmanned grain loading system and control method associated with a port hopper. This patent employs multi-sensor management and processing techniques to enhance operational efficiency and facilitate digitalization. The patent [DE 2001/19947739A1] describes a method and apparatus for loading bulk materials into mobile containers, including vehicles. The objective is to ascertain the container's dimensions through the use of a laser scanner to facilitate uniform loading and establish a specific unloading protocol.

The patent [SU 1986/1234326A1] pertains to the mechanization of loading processes. The system comprises a dosing device, hopper, and conveyor feeder for the loading of diverse bulk, granular, and lumpy materials. The patent CN 2019/110104460A pertains to a system designed for the loading and unloading of recyclable dust. The system comprises a silo, a dust screen, a primary discharge channel, a

dust conveyor, and several dust collection machines. The patent [CN 2024/118978035A] describes a movable, double-opening discharge hopper that is capable of weighing. The invention facilitates the discharge of material from a stationary location into a loading vehicle or directly from the vehicle.

The study utilises FEM (Finite Element Method) analyses to evaluate the theoretical calculations of the port loading bunker design, the static behavior of the bunker, and its dynamic behavior under the influence of various dynamic loads acting upon it. This contributes to the literature by examining structural analyses in a multifaceted manner, evaluating the dynamic performance of the system through modal analysis, and performing combined design, shear, and deflection checks for the steel columns and beams within the structural frame.

2. MATERIAL AND METHOD

The study conducted static and modal analyses on the ecologically designed port loading bunker (Figure 2), utilizing ideCAD finite element analysis to assess the loads impacting the structure.

The ecological port loading bunker, subject to static and dynamic analyses, features a volume of 100 m^3 and is mounted on a steel construction chassis approximately 5 m above ground. Its frame structure comprises a grid and Flex-Flax at the entrance of the internal chamber (Figure 3). Table 1 presents the design parameters of the ecological port loading bunker. The steel grades employed are St 37 and St 44.

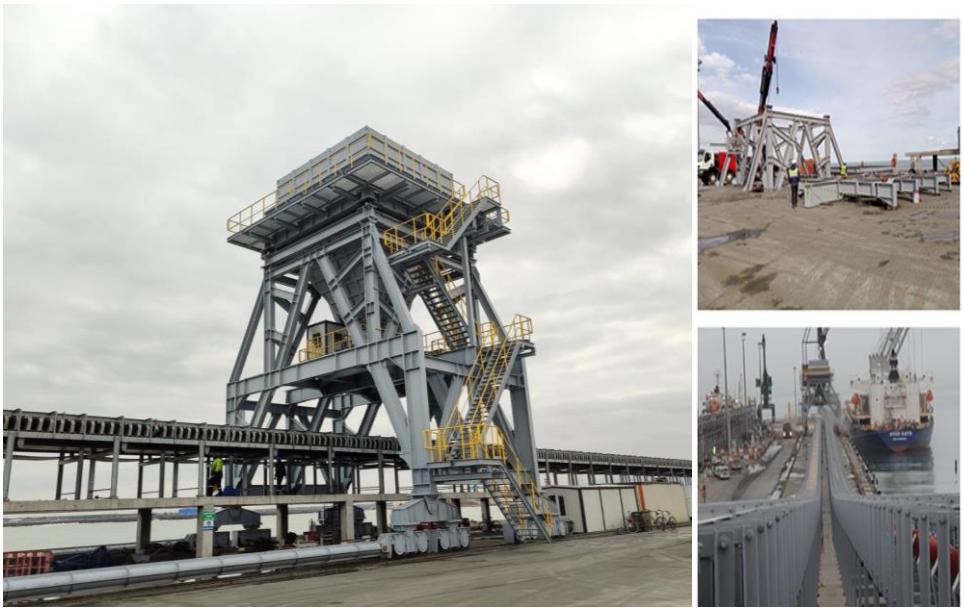

Figure 1. Ecological Port Loading Bunker

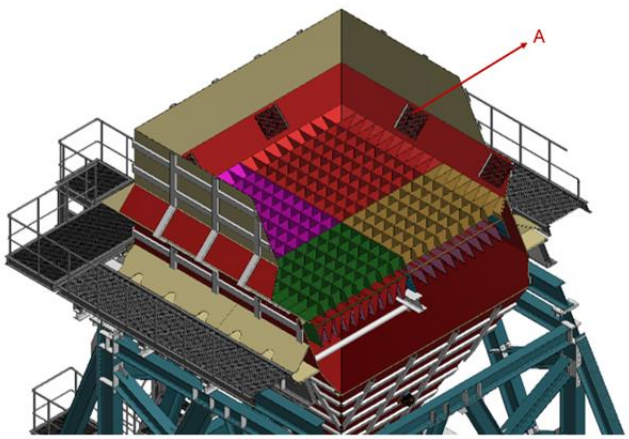

Figure 2. Angled Closure System (Flex-Flap)

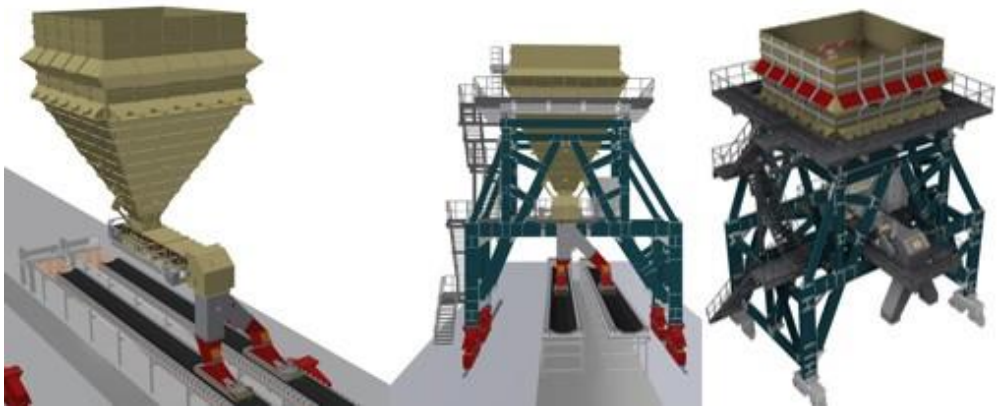

Figure 3. 3D Design of Ecological Port Loading Bunker

Table 1. Ecological Port Loading Bunker Design Parameters

Building Geometric Information	
Number Of Floors	1
Structure Height	11,56 (m)
The Height of the Structure Above the Rigid Basement	11,56 (m)
Rigid Basement Floor	0
Rigid Basement Floor Number	-1
Maximum Floor Height	11,56 (m)
Maximum Beam Clearance	0 (m)
Planned Use	
Number of Rigid Diaphragms	0

The comprehensive study of the system delineates the loads affecting it and various combinations of these loads, as seen in Table 2.

Table 2. Loading and Combination

Loading and Combination	
G	Constant load
Q	Moving load
G'	Constant load (Effective section stiffnesses used)
Q'	Moving load (Effective section stiffnesses used)
Ez(G)	Vertical earthquake
WX(+)	Wind loading in X direction
WX(-)	Wind loading in X direction
WY(+)	Wind loading in Y direction
WY(-)	Wind loading in Y direction

2.1.Static Analysis

Finite element analyses of the structure were conducted utilizing the IdeCAD and IdeaStatiCa software. Because the IdeCAD program assumes that the column-beam joints are completely rigid, Karayer et al. [15] used Idea Statica to analyze the connections between the columns and beams in the structure. The example below illustrates the analysis of a connection pertaining to the structure in our study. Figure 4 presents an example of a column-beam connection. Tables 3, 4, and 5 present the input data for the connection analysis.

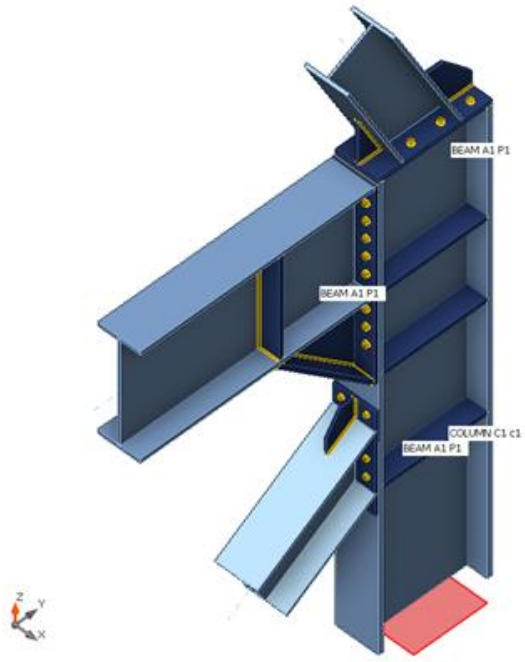

Figure 4. Column Beam Connection

Tension, shear, and bearing resistance calculations were carried out for a connection bolt in the column-beam connection shown in Figure 4 (e.g., B2) and verified in compliance with the Specification for Structural Steel Buildings (ANSI/AISC 360-22) [16].

Table 3. Geometry, Material and Support Description

Name	Cross-Section	Material	Support
COLUMN C1 c1	6 - HEB800	St 44	N-Vy-Vz-Mx-My-Mz
BEAM A1 P1	132 - HEA400		
BEAM A1 P1	139 - HEA800		
BEAM A1 P1	132 - HEA400		

Table 4. Bolts

Name	Bolt Assembly	Diameter [mm]	fu [MPa]	Gross Area [mm2]
M24 8.8	M24 8.8	24	800,0	452
M20 8.8	M20 8.8	20	800,0	314

Table 5. Load Effects (forces in equilibrium)

Name	Member	N [kN]	Vy [kN]	Vz [kN]	Mx [kNm]	My [kNm]	Mz [kNm]
LE1	COLUMN C1 c1	0,0	0,0	0,0	0,0	0,0	0,0
	BEAM A1 P1	5,0	0,0	13,0	0,0	-3,0	0,0
	BEAM A1 P1	215,0	0,0	49,0	0,0	-27,0	0,0
	BEAM A1 P1	496,0	0,0	3,0	0,0	-5,0	0,0

Detailed result for B2:

Tension resistance check (AISC 360-22 – J3-1)

$\phi R_n = \phi \cdot F_{nt} \cdot A_b = 203{,}4\ kN \geq F_t = 36{,}1\ kN$ *where:*

F_{nt} *=600 MPa – nominal tensile stress AISC 360-22 – Table J3.2*

$A_b = 452\ mm^2$ *– gross bolt cross-sectional area*

$\phi = 0.75$ *– resistance factor*

Shear resistance check *(AISC 360-22 – J3-1)*

$\phi R_n = \phi \cdot F_{nv} \cdot A_b = 152.7\ kN \geq V = 0.3\ kN;$ *where*

$F_{nv} = 450{,}4\ MPa$ *– nominal shear stress AISC 360-22 – Table J3.2*

$A_b = 452\ mm^2$ *– gross bolt cross-sectional area*

$\phi = 0.75$ *– resistance factor*

Bearing resistance check *(AISC 360-22 – J3-6)*

$R_n = 1,20 \cdot l_c \cdot t \cdot F_u \leq 2,40 \cdot d \cdot t \cdot F_u$

$\phi R_n = 371.2\ kN \geq V = 0.3\ kN;$ *where:*

$l_c = 38\ mm$ *clear distance, n the direction of the force, between the edge of the hole and the edge of the adjacent hole or edge of the material*

$t = 30\ mm$ *– thickness of the plate*

$d = 24\ mm$ *– diameter of a bolt*

$F_u = 360{,}0\ MPa$ *– tensile strength of the connected material*

$\phi = 0.75$ *– resistance factor for bearing at bolt holes*

Interaction of tension and shear check (AISC 360-22 – J3-2)

The required stress, in either shear or tension, is less than or equal to 30% of the corresponding available stress and the effects of combined stresses need not to be investigated.

The results from these calculations are presented in Table 6 (e.g., B2 in the first row), and the corresponding equivalent stress graph for this connection is illustrated in Figure 5.

Table 6. Bolts Analysis Results

Shape	Item	Grade	Loads	F_t [kN]	V [kN]	ϕR_n,bearing [kN]	Ut_t [%]	Ut_s [%]	Ut_{ts} [%]	Detailing	Status
	B2	M24 8.8 - 1	LE1	36,1	0,3	371,2	17,7	0,2	-	OK	OK
	B3	M24 8.8 - 1	LE1	25,1	0,4	466,6	12,3	0,3	-	OK	OK
	B4	M24 8.8 - 1	LE1	23,5	0,8	466,6	11,6	0,5	-	OK	OK
	B5	M24 8.8 - 1	LE1	20,5	1,3	466,6	10,1	0,8	-	OK	OK
	B6	M24 8.8 - 1	LE1	26,0	2,1	466,6	12,8	1,4	-	OK	OK
	...	...	...	...	...	...	...	...	...	...	...
	B35	M24 8.8 - 1	LE1	108,8	37,6	311,0	53,1	24,6	-	OK	OK
	B36	M24 8.8 - 1	LE1	163,6	38,1	311,0	80,5	25,0	-	OK	OK

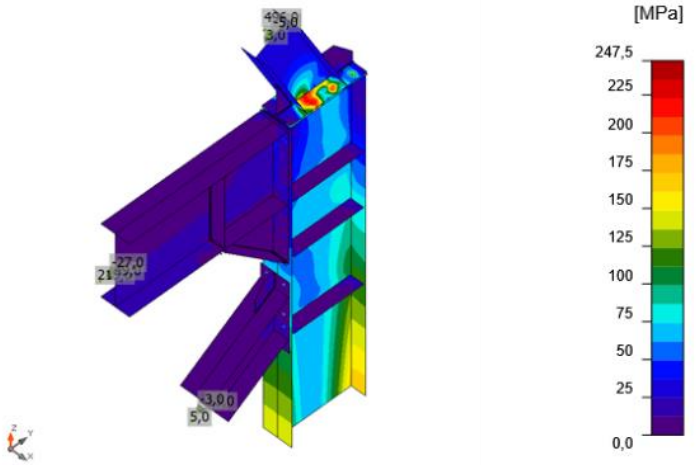

Figure 5. Equivalent stress, LE1

The static analyses conducted on the final design of the ecological port bunker included assessments of deflection, shear capacity, and composite design for the chassis steel beams; the resulting displacements and internal forces within the structure were evaluated.

St 44-St 37 has been specified as the material for the bunker structure and supplementary steel components. During design verification, it was determined that the structure was adequately designed when the PMM ratio (the ratio of the capacity demanded by a structural element to the available capacity of the cross-section) remained below 0.9 for the most critical load combinations of axial load and bending moments in opposing directions under its own weight (internal forces) (Figure 6), and subsequently when the bunker was fully loaded (under axial loads) to evaluate its static behavior (Figure 7). Total structural mass: 324.65 t.

Figure 6 illustrates the stresses generated in the chassis group, color-coded based on the percentage of the yield stress value of the steel material. The profiles experiencing the greatest stress are depicted in yellow in the illustration. The lack of red-colored profiles signifies that the construction is secure.

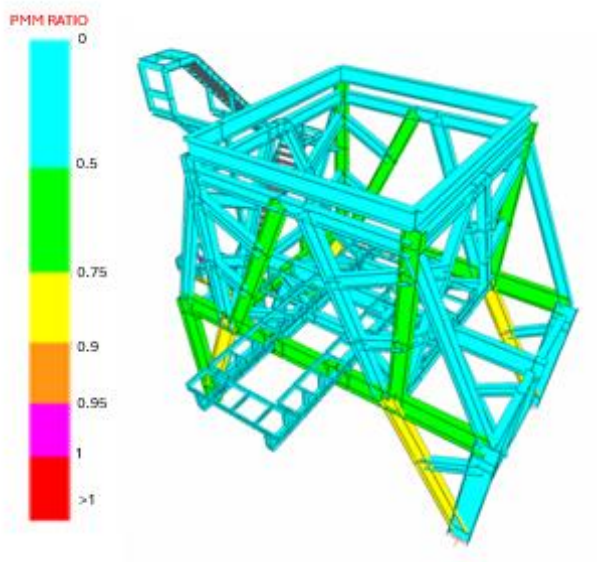

Figure 6. Stresses Induced by Its Own Weight

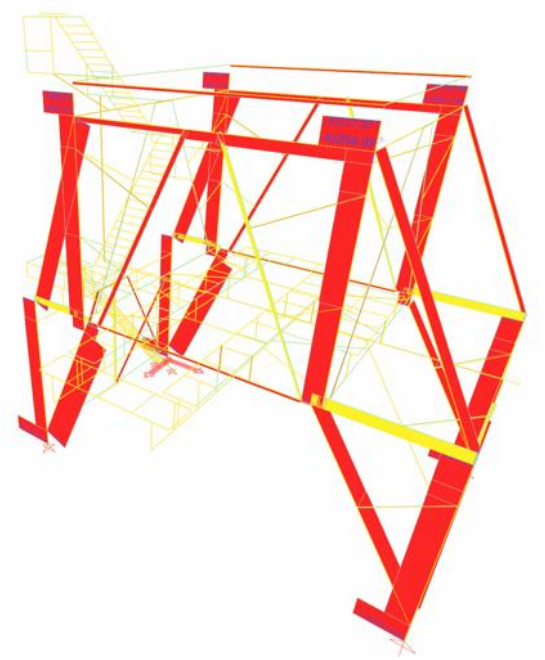

Figure 7. Axial loads in the vertical direction when the bunker is completely full

Figure 7 indicates that the bunker has a constant weight of 64 tonnes, whereas its weight when filled is 165.3 tonnes. The red color in the illustration denotes compressive forces, whereas the yellow color signifies tensile forces. Figure 8 illustrates the deformations in the structure resulting from external (wind) forces in the Y and X axes. The estimations of wind force took into account the average speed of the wind in the plant's surrounding area.

2.2. Modal Analysis

The targeted dynamic participation ratio indicates the contribution of a specific vibration mode to the total mass, facilitating the analysis of structural response to dynamic loads, including earthquakes. 'Modal Mass Participation Ratios' represent the fractions of the total mass of a structure that are affected by designated modes during an earthquake in a specific direction. These ratios aim to exceed a specified threshold (e.g., 95%). The analysis determined the minimum ratio for the total structure mass, establishing a maximum value of 0.95.

In the modal analysis, the structure's center of mass was displaced by 5% in the +Y, -Y, +X, and -X directions, and a dynamic analysis was carried out (Figure 9). For each analysis, the modal periods and frequencies, natural mass in degrees of freedom, modal participation factors, and modal mass participation ratios were calculated.

In the study, 45 modes were found, and eigenvalues and angular frequencies have been calculated to elucidate the dynamic behavior of the system utilizing modal frequency and period values. The system's natural frequency values were ascertained (Table 8).

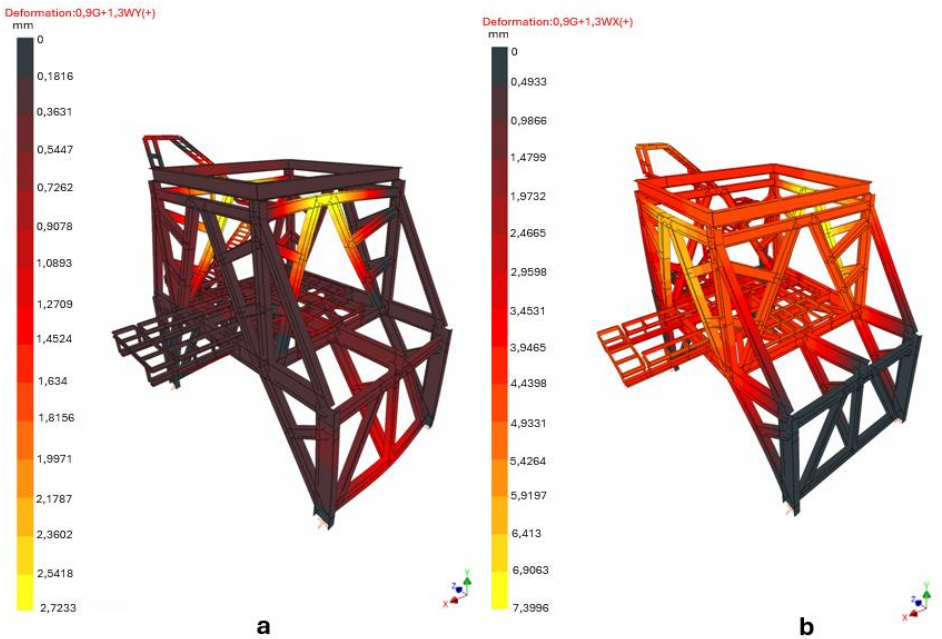

Figure 8. Structural Displacements Resulting from External Forces
a) along the Y axis b) along the X axis

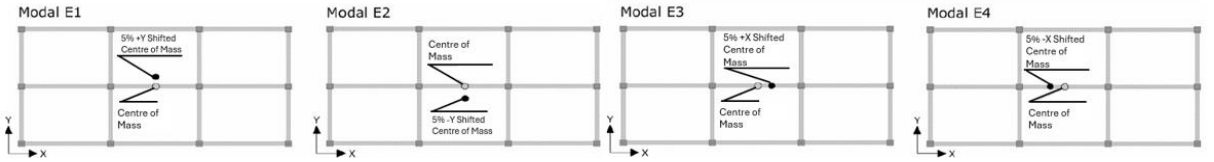

Figure 9. Shifting of the centre of mass in the X and Y directions

Table 7. Natural Masses in Degrees of Freedom

Ux [t]	Uy [t]	Uz [t]	Rx [tm²]	Ry [tm²]	Rz [tm²]
324,65163	324,65163	0	0	0	5723,81872

Table 8. Modal Period and Frequency

Mod	Period [s]	Frequency	Angular Freq. [rad/s]	EigenValue [rad²/s²]
1	0,54770	1,82582	0,2002	0,040
2	0,30417	3,28761	0,3605	0,130
3	0,21534	4,64386	0,5093	0,259
4	0,20137	4,96592	0,5446	0,297
5	0,15927	6,27868	0,6885	0,474
.....	.....	.....	.....	.....
44	0,01053	94,99400	10,4173	108,519
45	0,00913	109,57314	12,0160	144,385

The modal participation factor, calculated individually for each mode, illustrates the interaction between the mode shape and the mass distribution, as well as the potential for movement in response to external excitation (Table 9).

Modal participation factors are used to calculate modal mass participation ratios (Table 10). This ratio indicates what percentage of the total mass is activated by a specific mode. In earthquake regulations (e.g., Turkish Building Earthquake Regulation—TBDY), the number of modes to be considered in dynamic analysis is subject to the condition that the total modal effective mass participation ratio reaches at least 90% (or 95% in some regulations) in both horizontal earthquake directions. This ensures that the analysis covers all important vibration behaviors of the structure.

3. RESULTS

This research presents the design and production of an "Ecological Port Loading Bunker," which significantly influences national and international trade in bulk commodities across sectors including mining, aggregates, ore, agriculture, and grain. This study includes all calculations pertinent to the developed ecological bunker. It encompasses theoretical calculations, the static behavior of the bunker, its response to dynamic loads (such as moving loads, vertical seismic loads, and wind loads), and an analysis of the system's dynamic performance through modal analysis of the structural system. Additionally, a comprehensive design assessment of the steel columns and beams within the structural frame has been conducted.

The static analysis examined the stresses and deformation patterns that may arise in the structure under static and dynamic loads. Consequent to the dynamic analysis, comprehensive design verifications, shear capacity assessments, and deflection evaluations were conducted and documented for each column and beam inside the structure under the most adverse load combinations possible.

The safety of the structure was assessed by integrated design checks, verifying that the ratio of estimated axial, major axis bending, and minor axis bending values to the permitted strength value was below 1, with findings presented in Table 11. The shear capacity assessment revealed that the ratio of the load value (ϕ) imposed on the structure under unfavorable load combinations to the maximum load value (ϕ) that the beam/column can withstand is less than 1, and this has been documented. Table 12 presents the load values and the /ϕ ratio, whereas Table 13 displays the deflection check data. In beam deflection control, the deflection limit (sudden deflection limit value induced by moving loads) is established according to the ratio of the beam span (ln) to 360. The calculations conducted throughout the analysis verified that the service loads applied on the beam adhered to the deflection limit value.

Table 9. Modal Participation Factor

Mod	Period [s]	Ux [t]	Uy [t]	Uz [t]	Rx [tm²]	Ry [tm²]	Rz [tm²]
1	0,54770	13,60145	0,00387	0	0	0	0,57374
2	0,30417	1,40243	0,22182	0	0	0	-0,01866
3	0,21534	0	-1,26291	0	0	0	-0,04395
4	0,20137	-0,02672	13,98002	0	0	0	-0,91794
5	0,15927	0,06946	-0,21183	0	0	0	-0,07774
.....	.....	.....	.....	.....	.....	.....	.....
44	0,01053	-1,86648	-3,58732	0	0	0	-8,98001
45	0,00913	-0,30664	-0,95760	0	0	0	33,45701

Table 10. Modal Mass Participation Ratio

Mod	Period [s]	Ux [t]	Uy [t]	Uz [t]	Top Ux	Top Uy	Top Uz	Rx [tm²]	Ry [tm²]	Rz [tm²]	Top Rx	Top Ry	Top Rz
1	0,54770	0,56984	0,00000	0,00000	0,56984	0,00000	0,00000	0,00000	0,00000	0,00006	0,00000	0,00000	0,00006
2	0,30417	0,00606	0,00015	0,00000	0,57590	0,00015	0,00000	0,00000	0,00000	0,00000	0,00000	0,00000	0,00006
3	0,21534	0,00000	0,00491	0,00000	0,57590	0,00506	0,00000	0,00000	0,00000	0,00000	0,00000	0,00000	0,00006
4	0,20137	0,00000	0,60200	0,00000	0,57590	0,60707	0,00000	0,00000	0,00000	0,00015	0,00000	0,00000	0,00021
5	0,15927	0,00001	0,00014	0,00000	0,57591	0,60720	0,00000	0,00000	0,00000	0,00000	0,00000	0,00000	0,00021
.....	.....	.....	.....	.....	.....	.....	.....	.....	.....	.....	.....	.....	.....	.....
44	0,01053	0,01073	0,03964	0,00000	0,98344	0,97189	0,00000	0,00000	0,00000	0,01409	0,00000	0,00000	1,07857
45	0,00913	0,00029	0,00282	0,00000	0,98373	0,97471	0,00000	0,00000	0,00000	0,19556	0,00000	0,00000	1,27413

Table 11. Integrated design checks

Beam	Design Point [m]	Axial		Major Axle Bending		Minör Axle Bending		Control
		P_u [kgf]	$\phi * P_n$ [kgf]	M_u [kgf]	$\phi^* M_n$ [kgf]	M_u [kgf]	$\phi^* M_n$ [kgf]	Ratio <1
BEZ001 (HE 500 A) 1,2G+Q-Ex-0,3Ey+0,3Ez	2,89	-4073,73	426448,39	-12077,27	99666,40	-692,45	26715,11	0,15
BEZ002 (HE 600 A) 1,2G+Q-Ex-0,3Ey+0,3Ez	7,50	-16072,11	484738,62	-18881,16	132366,65	3161,61	29166,84	0,27
BEZ003 (HE 400 A) 1,2G+Q-Ex-0,3Ey+0,3Ez	0,08	-26211,52	310178,71	4443,72	60982,42	-859,06	22029,70	0,15
BEZ004 (HE 400 A) 1,2G+Q-Ex-0,3Ey+0,3Ez	0	-28023,73	310178,71	-5231,48	60982,42	-37,41	22029,70	0,13
BEZ005 (HE 500 A) 0,9G-Ex-0,3Ey-0,3Ez	0	-5406,62	426448,39	-2511,83	99666,40	-1644,92	26715,11	0,09
.....	.....	.....	.....	.....	.....	.....	.....	
BEZ418 (HE 200 B) 1,2G+Q-Ey-0,3Ex+0,3Ez	1,01	-1717,14	114379,72	39,80	14709,59	0	7718,20	0,01

Table 12. Shear capacity control

Beam	V_u [kgf]	$\phi * V_n$ [kgf]	Control $V_u/(\phi * V_n)$ <1
BEZ001 (HE 500 A) 1,2G+Q+Ex+0,3Ey+0,3Ez	21384,76	98932,87	0,216
BEZ002 (HE 600 A) 1,2G+Q+Ex+0,3Ey+0,3Ez	28906,91	129050,19	0,224
BEZ003 (HE 400 A) 1,2G+Q+Ex+0,3Ey+0,3Ez	2360,41	72180,61	0,033
BEZ004 (HE 400 A) 1,2G+Q-Ex-0,3Ey+0,3Ez	-2091,51	72180,61	0,029
BEZ005 (HE 500 A) 1,2G+Q+Ex+0,3Ey+0,3Ez	15528,25	98932,87	0,157
.....			
BEZ418 (HE 200 B) 1,4G	80,44	30285,57	0,003

Table 13. Deflection control

Beam	ln [m]	δ_i [mm]	Control δ_i<limit
BEZ001 (HE 500 A) G+Q	3	0,058	0,1<8,0 (l/360)
BEZ002 (HE 600 A) G+Q	3	0,050	0,1<8,7 (l/360)
BEZ003 (HE 400 A) G+Q	5	0,039	0,0<13,3 (l/360)
BEZ004 (HE 400 A) G+Q	5	0,046	0,0<13,5 (l/360)
BEZ005 (HE 500 A) G+Q	3	0,049	0,0<8,0 (l/360)
.....			
BEZ418 (HE 200 B) G+Q	2	0,010	0,0<5,6 (l/360)

4. DISCUSSION

The Ecological Port Loading Bunker proposed includes:
Enclosed Conveying Systems: Utilize fully enclosed systems, including covered belt conveyors, pneumatic systems, or enclosed screw conveyors, to transport bulk commodities to and from the bunker, therefore reducing dust emissions during transit.

Sealed Transfer Points (Drop Points): All locations where material is transported from one piece of equipment to another (e.g., conveyor to bunker) must be dust-tight, employing seals, flexible connectors, or dead boxes that compel the material to descend onto a settled layer, therefore minimizing drop height and impact velocity.

The dust extraction system to be incorporated in the subsequent phase of the project will be an air extraction system that removes air from within the bunker and collects it. Upon the pile's descent into the bunker, the air volume will alter, and the air will undergo purification through a succession of external jet-pulse filters. Initial design efforts pertaining to this feature have been conducted within the project timeline. The project is amenable to additional development and acts as a basis for forthcoming research and development initiatives. One of the developmental objectives to be implemented after project completion is to reduce dust dispersion by 85%–90% in a traditional bunker [17] by installing a filter-assisted suction system in the gaps. (“A” in Figure 2).

REFERENCES

1. Port Technology, 2016. What is a Smart Port? Available at: https://www.porttechnology.org/news/what_is_a_smart_port [Accessed 21 June 2019].
2. European Parliament and Council, 2011. DIRECTIVE 2011/92/EU OF THE EUROPEAN PARLIAMENT AND OF THE COUNCIL. Available at: https://eur-lex.europa.eu/eli/dir/2011/92/oj/eng.
3. Yorulmaz, M. and Patruna, E., 2022. Assessment of Sustainable Green Port Perception and Management. IJAR, 7(13), pp.148–168. doi:10.47356/ijar.2022.68612.1012468.
4. Mısır, G. and Laman, M., 2020. Numerical Modelling of Full-Scale Lateral Load Test. Avrupa Bilim ve Teknoloji Dergisi, (18), pp.454–464. doi:10.31590/ejosat.695194.
5. Yılmaz, N., 2018. Wind Climate, Wave Climate, and Current Regime Modeling in Samsun Bay Coastal Waters. Journal of the Faculty of Engineering and Architecture of Gazi University, 33(1), pp.279–297. doi:10.17341/gazimmfd.406801.
6. Briassoulis, D., 1998. Silos: Fundamentals of Theory, Behaviour and Design. 1st ed. Taylor & Francis.
7. Aoyama, S. and Okwach, S., 1991. Mechanical behavior of a single storage silo under grain pressure. Transactions of the Japanese Society of Irrigation, Drainage and Reclamation Engineering, 156, pp.81–92.
8. Wojcik, M., Enstad, G.G. and Jecmenica, M., 2003. Numerical Calculations of Wall Pressures and Stresses in Steel Cylindrical Silos with

Concentric and Eccentric Hoppers. Particulate Science and Technology, 21(3–4), pp.247–258. doi:10.1080/02726350307486.
9. Brown, C.J., 2008. Developments in the design of rectangular plan form silos. In Proceedings of The International Conference on Structures and Granular Solids: From Scientific Principles to Engineering Applications. The Royal Society of Edinburgh, Scotland, UK, pp.103–111.
10. Gençay, E., 2025. Analysis and Comparison of a Reinforced Concrete Building with Package Programs Used in Civil Engineering. Bilecik Seyh Edebali University Journal of Science, 12(1), pp.01–08. doi:10.35193/bseufbd.1363036.
11. Shen, J., Jin, C., Yuan, J., Cai, Y. and Wheeler, C., 2023. Experimental and numerical analysis of hopper dust suppression during discharge of free falling bulk solids. Powder Technology, 415, p.118108. doi:10.1016/j.powtec.2022.118108.
12. Colinet, J.F., Cecala, A.B. and Patts, J.R., 2018. Dust Suppression Hopper: reduces dust liberation during bulk loading: Two case studies. Mining Engineering, 70(9), pp.41–46.
13. Zhang, H., Meng, W., Zhang, B., Yuan, Y., Yin, X. and Zhao, X., 2024. Flow Field Characteristics of Fugitive Dust from Grab Unloading in an Open Space. Processes, 12(1), p.49. doi:10.3390/pr12010049.
14. Vaicis, I., Janushevskis, A., Viksne, I. and Auzins, J., 2019. Analysis and optimization of dust control hopper system. In Proceedings of the 14th International Conference on Vibration Problems 2019, pp. 1157–1163.
15. Karayer, A. and Severcan, M.H., 2018. Comparing and analysing of different type reinforced concrete structures with package programs. Black Sea Journal of Engineering and Science, 1(2), pp.41–50.
16. American Institute of Steel Construction, 2022. Specification for Structural Steel Buildings (ANSI/AISC 360-22). Chicago, IL: American Institute of Steel Construction.
17. Pulse Type Bag Filter of Eco Hooper Avaliable at: https://www.gbm-industry.com/eco-hopper/?keyword=samson%20eco%20hopper&matchtype=p&gad_source=1&gad_campaignid=13663854898&gbraid=0AAAAACmqKWst79yidqi-adr-ff-c6sbwb&gclid=EAIaIQobChMIzcCkoJWhkQMVYhkGAB2m2TjmEAAYASAAEgLG6fD_BwE